AIAA JOURNAL
Vol. 43, No. 3, March 2005

Antialiasing Filters for Coupled Reynolds-Averaged/ Large-Eddy Simulations

J. U. Schlüter* and H. Pitsch†
Stanford University, Stanford, California 94305-3030

The increasing complexity of engineering problems makes the coupling of multiple simulation codes attractive. In fluid mechanical applications, the physical range of flow phenomena that can be modeled can be extended significantly by coupling flow solvers based on the Reynolds-averaged Navier–Stokes (RANS) approach and on large-eddy simulations (LES). These separate flow solvers run simultaneously and exchange information at the interface. However, because the LES flow solver operates usually with a much smaller time step, the LES data have to be sampled to provide data for the RANS flow solver. In the sampling process, aliasing errors can occur. Possibilities are investigated to suppress aliasing errors while preserving the amplitude and phase of the long wave spectrum.

Nomenclature

a_m, b_n	=	filter constants
D	=	diameter of the pipe
f	=	frequency
$H(\lambda)$	=	desired filter response
N, M	=	order of the filter
Re	=	Reynolds number
$r(t_k)$	=	filter response on the discrete time t_k
S	=	swirl number
Sr	=	Strouhal number
$s(t_k)$	=	original signal on the discrete time t_k
t	=	time on the large-eddy-simulation timescale
u_c	=	convective velocity
u_x, u_r, u_ϕ	=	velocity components in axial, radial, and azimuthal direction
x, r, ϕ	=	coordinates in axial, radial, and azimuthal direction
x_0	=	location of the interface point
λ	=	nondimensional frequency
τ	=	time on the Reynolds-averaged Navier–Stokes timescale

I. Introduction

CURRENTLY, a wide variety of flow phenomena are addressed with numerical simulations. Many flow solvers are optimized to simulate a limited spectrum of flow effects effectively, such as single parts of a flow system, but are either inadequate or too expensive to be applied to a very complex problem.

As an example, the flow through a gas turbine can be considered. In the compressor and the turbine section, the flow solver has to be able to handle the moving blades, model the wall turbulence, and predict the pressure and density distribution properly. This can be done by a flow solver based on the Reynolds-averaged Navier–Stokes (RANS) approach (see Ref. 1). On the other hand, the flow in the combustion chamber is governed by large-scale turbulence, chemical reactions, and the presence of fuel spray. Experience shows that these phenomena require an unsteady approach.[2] Hence, for the combustor the use of a large-eddy simulation (LES) flow solver is desirable.[3]

Although many design problems of a single flow passage can be addressed by separate computations, only the simultaneous computation of all parts can guarantee the proper prediction of multicomponent phenomena, such as compressor/combustor instability and combustor/turbine hot-streak migration. Therefore, a promising strategy to perform full aerothermal simulations of gas turbine engines is the use of a RANS flow solver for the compressor section, an LES flow solver for the combustor, and again a RANS flow solver for the turbine section (Fig.1).

The approach to couple simulation codes has already been used in other areas of application, most notably in global climate simulations,[4] and recently found more attention in the engineering community.[5] However, the idea to couple RANS and LES flow solvers is a very recent approach. It is a unique method to construct an LES/RANS hybrid. Whereas other LES/RANS hybrid approaches, such as detached-eddy simulations[6] and limited-numerical scales[7] combine LES and RANS in a single flow solver, the approach to couple two existing flow solvers has not only the distinct advantage to build on the experience and validation, but also the numerical methods and specific optimization that has been put into the two codes during their development.

A demonstration for an applied coupled RANS/LES computation is the simulation of the flow development downstream of the final compressor stage into a diffuser of a gas turbine engine[8] shown in Fig. 2. The interactions between the compressor and the prediffuser of the combustor can be studied. Here, the compressor stage is computed with a RANS flow solver because the wall-bounded flows around the stator and the moving rotor can be efficiently predicted with this approach. The diffuser on the other hand is computed with an LES flow solver because only this approach can assure the accurate prediction of detachments in this portion of the flow. The flow solvers are two-way coupled, which means that both flow solvers communicate the flow information at the interface to the peer flow solver.

To ensure the information transfer of flow properties and the correct specification of boundary conditions in such complex applications, validation studies have to be performed. Whereas recent work focused on boundary conditions, the present work will investigate the preservation dynamic properties of the data exchange. It will demonstrate the presence of aliasing and will present strategies to attenuate the aliasing error.

II. Interface Conditions

The simultaneous computation of the flow in all parts of a gas turbine using multiple flow solvers requires an exchange of information at the interfaces of the computational domains of each part.

Received 7 August 2003; presented as Paper 2004-0258 at the 42nd Aerospace Sciences Meeting, Reno, NV, 5–8 January 2004; revision received 24 September 2004; accepted for publication 12 October 2004.

*Research Associate, Center for Turbulence Research. Member AIAA.
†Assistant Professor, Center for Turbulence Research. Member AIAA.

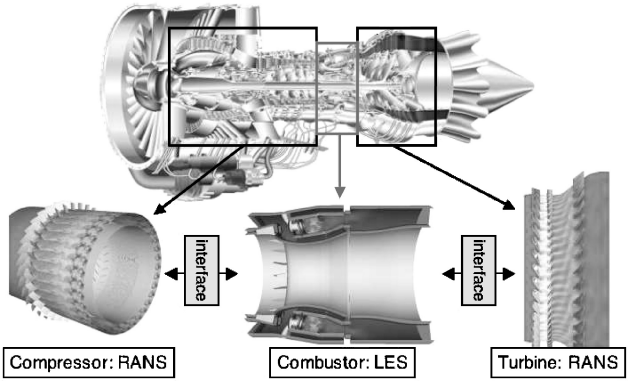

Fig. 1 Decomposition of gas turbine engine (RANS/LES of compressor/diffuser,[8] LES of combustor,[3] RANS of turbine section[1]).

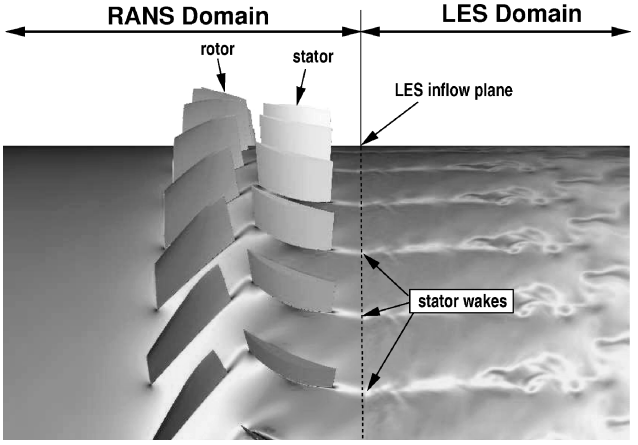

Fig. 2 Example of a two-way coupled RANS/LES: compressor stage and a prediffuser in a gas turbine.[8]

Previous work has established algorithms that ensure that two or more simultaneously running flow solvers are able to exchange the information at the interfaces efficiently.[9–11]

The necessity of information exchange in the flow direction from the upstream to the downstream flow solver is obvious: The flow in a passage is strongly dependent on mass flux, velocity vectors, and temperature at the inlet of the domain. However, because the Navier–Stokes equations are elliptic in subsonic flows, the downstream flow conditions can have a substantial influence on the upstream flow development. This can easily be imagined by considering that, for instance, a flow blockage in the turbine section of the gas turbine can determine and even stop the mass flow rate through the entire engine. This means that the information exchange at each interface has to go in both downstream and upstream directions.

When an LES flow solver computing the flow in the combustor is considered, information on the flowfield has to be provided to the RANS flow solver computing the turbine as well as to the RANS flow solver computing the compressor, while at the same time the LES solver has to obtain flow information from both RANS flow solvers (Fig. 3). The coupling can be done using overlapping computational domains for the LES and RANS simulations. For the example of the compressor/combustor interface, this would imply that inflow conditions for LES will be determined from the RANS solution at the beginning of the overlap region, and correspondingly, the outflow conditions for RANS are determined from the LES solution at the end of the overlap region.[8]

However, the different approaches to turbulence modeling used by the different flow solvers make the coupling of the flow solvers challenging. Because LES resolves large-scale turbulence in space and time, the time step between two iterations is relatively small. RANS flow solvers average all turbulent motions over time and predict ensemble averages of the flow. Even when a so-called unsteady

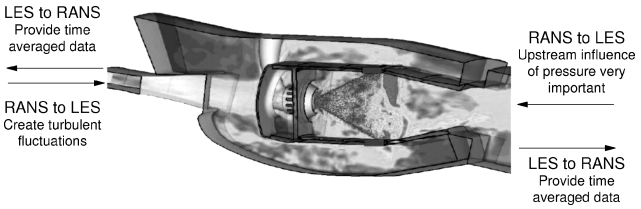

Fig. 3 Gas turbine combustor with interfaces.

RANS approach is used, the time step between two ensemble averages of the RANS flow solver is usually larger by at least one order of magnitude than that of an LES flow solver.

To provide boundary conditions for the RANS flow solver from the LES solution, the data have to be averaged or filtered in time, and an appropriate down-sampling technique has to be developed. For a statistically stationary flow, we have shown in the past that a time average of the data over a time period larger than the integral timescale of the turbulence provides sufficiently accurate and constant RANS boundary conditions. However, this type of sampling process will introduce errors if full-scale hydrodynamic oscillations occur. For the simple time-averaging method, the transmission of these oscillations across the interface results in a phase-delay and aliasing errors, which will lead to a change in frequency and, hence, possibly to the attenuation or forcing of instabilities.

As an analogy, the digitization of a continuous signal during the acquisition of experimental data can be considered. Here, the highest frequency recorded without error is the Nyquist frequency, defined as half of the sampling frequency. Experimentalists use low-pass filters to remove high-frequency disturbances before the sampling process. Omitting the filtering would result in aliasing errors, which means that underresolved frequencies, $f > f_{\text{Nyquist}}$, appear as low-frequency contributions in the long-wave spectrum. Hence, low-pass filtering before to the digitization is necessary.

For the communication between LES and RANS flow solvers, a similar procedure has to be developed to avoid aliasing of frequencies in the sampling of the LES data. The current study investigates the use of filters to ensure the communication of dynamic properties, such as the frequency, the amplitude, and the phase of a given perturbation.

III. Test Case and Flow Solver

For this investigation, a pipe flow is computed by using two fully coupled flow solvers, one computing the upstream and the other computing the downstream part of the pipe. For simplicity and to focus on the issue of aliasing, we will first consider a laminar flow at a pipe Reynolds number $Re = 10^3$. A fully turbulent flow will be considered. Then, there is no difference in using an LES or RANS flow solver, and the same code can be used for both portions. However, to represent a flow simulation, where LES is used for an upstream and RANS for a downstream portion of the flow domain, the downstream flow solver will be run with a much larger time step. To study the transfer of dynamic properties from the upstream to the downstream flow solver, the inflow of the upstream portion of the pipe is perturbed periodically. Aliasing may then occur when the temporally highly resolved solution of the upstream domain has to be sampled to provide data at the time step of the downstream flow solver.

Figure 4 shows the considered test case: A pipe is split into an upstream domain computed by one flow solver and a downstream domain computed by the second. Both pipe segments are 3 diameters D long with an overlap of $1D$. An interface is used to communicate the flow variables between both flow solvers.[11]

The inflow of the upstream pipe is defined as a laminar parabolic inflow in the axial direction and a parabolic profile in the azimuthal direction, thus, simulating a laminar swirling pipe flow. The swirl number of this flow is $S = 0.15$, where

$$S = \frac{1}{D}\frac{\int_0^D r^2 \bar{u}_x \bar{u}_\phi \, \mathrm{d}r}{\int_0^D r \bar{u}_x^2 \, \mathrm{d}r}$$

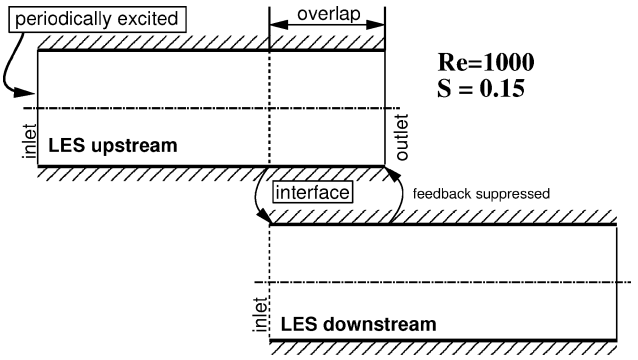

Fig. 4 Geometry of test case.

with u_x the axial velocity component and u_ϕ the azimuthal velocity component. To create a wave that is convected with a constant bulk velocity, the azimuthal velocity component has been modulated by

$$\bar{u}_\phi(t) = \bar{u}_{\phi,\text{mean}} \cdot [1.0 + 0.3 \cdot \sin(2\pi \cdot Sr \cdot t)] \tag{1}$$

with $\bar{u}_{\phi,\text{mean}}$ the mean azimuthal velocity for $S = 0.15$ and Sr the Strouhal number defined as $Sr = fD/U_{\text{bulk}}$. The modulated swirl travels down the pipe where it is getting sampled.

The choice was made to modulate the swirl velocity rather than the axial velocity because this simulates a convective wave without changing temporarily the bulk velocity.

For the current investigation, a structures LES flow solver has been used.[12] The filtered momentum equations are solved with a low Mach number assumption on an axisymmetric structured mesh. A second-order finite volume scheme on a staggered grid is used.[13] The subgrid stresses are obtained by a dynamic procedure.[14,15]

For the real-time exchange of flow variables during the simultaneous computation of both domains, a special interface software has been used.[9,10] The interface establishes a communication between the two flow solvers for the exchange of flow variables after a given time step $\Delta\tau$. At that time, each of the flow solvers obtains a set of flow variables for each point at the interface. Then, each flow solver evaluates the interface boundary conditions on the basis of the obtained data. For the downstream solver, the velocity data obtained from the upstream solver can directly be specified as inlet condition.

The LES boundary condition at the outlet of the upstream flow solver can be defined using a body force to drive the solution near the outlet to the desired flowfield.[16] However, for the present case, no such body force is employed, which means that the feedback from the downstream flow solver to the upstream flow solver is suppressed. This is done to ensure that aliased frequencies in the downstream domain are not transferred back to the upstream domain, where they would be able to compromise the original signal. Although initial tests with a true two-way coupling did not show such an effect, the feedback has been suppressed to demonstrate clearly that downstream aliased frequencies have not been present in the upstream domain. Because there is no feedback from the downstream flow solver, the time-evolving solution of the upstream flow solver is identical for all cases reported here.

IV. Aliasing

To demonstrate the presence of aliasing, the upstream flow is periodically excited and the transfer of these frequencies to the downstream flow solver examined. The periodic excitation is carried out simultaneously with two frequencies. These frequencies are chosen such that the lower one is resolved by the time step of the downstream flow solver, and the higher frequency is underresolved. In real applications, the high-frequency perturbation corresponds to high-frequency turbulence that is resolved in LES domain, but not in the RANS domain. The low-frequency perturbation corresponds to large-scale motions of the flow that are resolved by LES and RANS.

The two excitation frequencies are at Strouhal numbers $Sr = 1.0$ and $Sr = 7.5$. The interface frequency, defined by the chosen RANS time step, $f_{\text{interface}} = 1/\Delta\tau$, is set to $Sr = 10.0$, which leads to a Nyquist frequency of $Sr = 5.0$. Hence, the low frequency at $Sr = 1.0$ is well resolved and can be transferred to the downstream domain. However, the higher frequency is underresolved and will lead to aliasing.

To quantify the transfer of the dynamic properties, the transient data are recorded for several points over 50 periods of the lower frequency, $Sr = 1.0$, and analyzed. The points are located on the $x = 2D$ plane. For the upstream flow solver, the points are just in the same location, where the data are acquired for the downstream flow solver. The points are at the same location, where the data for the downstream flow solver have to be specified. In the following discussion, data for the point $x = 2D$, $r = 0.5R$, and $\phi = 0$ will be presented.

The transient data are analyzed by a Fourier transform of the kinetic energy to assess the spectral characteristics. Figure 5 shows the energy spectrum in the upstream domain. Because we are considering a laminar flow, the spectrum is very smooth and shows mainly the two distinct peaks resulting from the forcing of the flow. There are some additional smaller peaks from the folding of the two frequencies (such as $Sr = 8.5$ and $Sr = 6.5$) and subharmonic responses of the flow (such as $Sr = 2.0$). The goal of a successful signal processing is to transfer the long-wave frequency, $Sr = 1.0$, with no energy loss, while suppressing the high-frequency disturbance, $Sr = 7.5$.

Figure 6 shows the energy spectrum for the same physical point, but in the downstream domain. Because the flow solver computing the upstream domain has transferred the signal without any special anti-aliasing, the high-frequency perturbation in the upstream domain has been aliased and can be found now in the long-wave spectrum at $Sr = 2.5$.

This may cause considerable problems because this frequency is resolved by any unsteady RANS flow solver operating at a time step corresponding to the interface frequency. Because the peak in the long-wave spectrum at $Sr = 2.5$ is not present in the upstream domain, it is obvious that this error has been introduced entirely by the sampling process. To suppress the high-frequency perturbation, the upstream flow solver has to treat the signal during the sampling process in a way that the aliasing is removed and both amplitude and phase of the low-frequency oscillation is preserved.

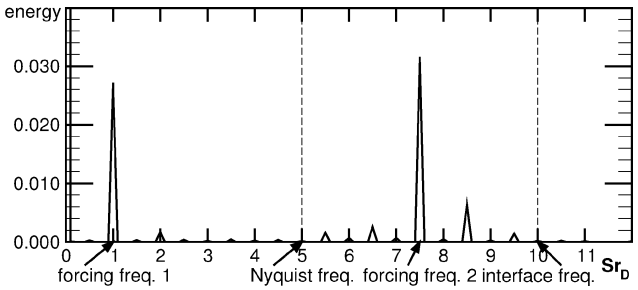

Fig. 5 Energy spectrum at point $x = 2D$, $r = 0.5R$, and $\phi = 0$ in interface plane of upstream domain.

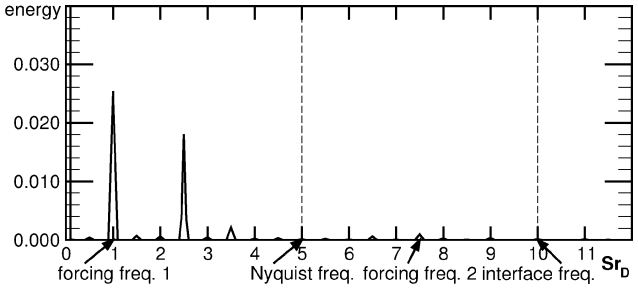

Fig. 6 Energy spectrum at interface plane of downstream domain; physically identical point as Fig. 5 ($x = 2D$, $r = 0.5R$, and $\phi = 0$), no filter.

V. Temporal Filters

A. Definition

A common procedure to avoid aliasing errors in experiments is to use low-pass filters before the sampling process. The low-pass filter suppresses all frequencies above the Nyquist frequency while letting all lower frequencies pass. This filtering process has to be done before the sampling process because otherwise the aliasing error has already taken effect and is indistinguishable from the rest of the long-wave spectrum.

Using the same strategy for the sampling of LES data leads to the need of an appropriate digital filter. A digital filter can be defined as

$$r(t_k) = \sum_{n=0}^{N} b_n s(t_{k-n}) + \sum_{m=1}^{M} a_m r(t_{k-m}) \tag{2}$$

with r the filter response, s the original signal, and t_k the time, where $t_k - t_{k-1}$ is the LES time step Δt. Because in LES computations the time step is usually not constant, but varies to maintain the highest possible time step that satisfies the Courant–Friedrichs–Lewy condition, a presampling process has to be made. This presampling averages the data with a higher frequency than the actual sampling frequency. To avoid aliasing in the presampling process, the frequency of the presampling has to be chosen well within the energy decay of a turbulent energy spectrum, so that the energy of frequencies higher than the Nyquist frequency are considerably smaller than the energy of the lower frequencies. A filter such as Eq. (2) can then be applied.

A filter in the form of Eq. (2), a so-called infinite impulse response filter, uses the history of the signal and the history of prior filter responses to define the filter. However, a simplified filter that uses only the history of the signal, a so-called finite impulse response filter (FIR filter), may have advantages. This filter is given in the form

$$r(t_k) = \sum_{n=0}^{N} b_n s(t_{k-n}) \tag{3}$$

First, FIR filters are always stable. Because of the absence of the filter response, no feedback is possible, and hence, this kind of filter is unable to amplify errors. Second, FIR filters have a linear phase response. The advantage of this will be made clear later.

Because of the high number of points at the interface that the filter has to be applied to, the order N of the filter is sought to be small inasmuch as N determines the number of time steps that have to be recorded.

For the current investigation, two different filters have been used. The detailed description of the determination of the filter constants may be found in the Appendix.

One filter is based on the Fourier series method (FSM), which is the exact solution for an infinite number of filter coefficients for a chosen filter response $H(\lambda)$. The filter response of this filter is shown in Fig. 7. The dashed line denotes the ideal filter response, which is equal to one below the cutoff frequency and otherwise zero. Because only a limited number of filter coefficients are available, the actual filter response differs from the ideal filter.

The order of the filter is chosen to be $N = 21$. This order is the lowest order ensuring a filter response of unity at 0 Hz and, thus, ensuring mean momentum conservation. The low order of the filter results in an overshoot right next to the cutoff frequency, which is known as Gibb's phenomenon.

The second filter employed attempts to minimize this effect. Window functions can be used to smoothen the ripple effects. Here, the usage of a Kaiser window is proposed, resulting in a smoothed filter response (Fig. 8).

B. Temporal Filter: Amplitude Response

In the next step, the filters are applied to the results of the computation of the upstream domain. Two simulations are performed, with one using the FSM filter and the other the Kaiser window. The signal response of both computations using the two different filters

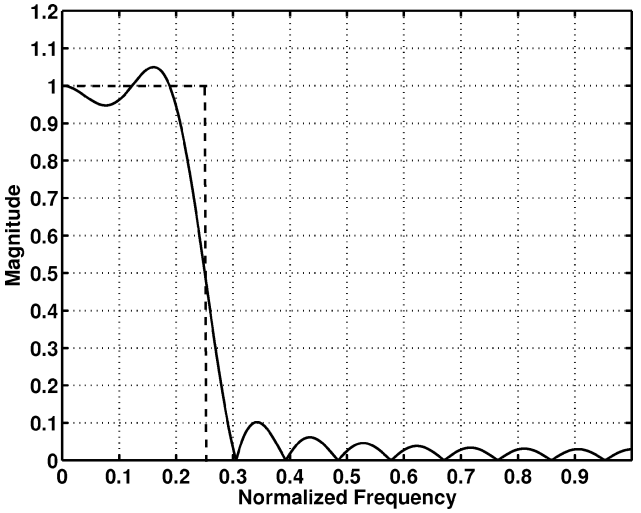

Fig. 7 $N = 21$, **cutoff frequency = 0.25: – – –, ideal filter response and ——, filter response of filter designed with FSM.**

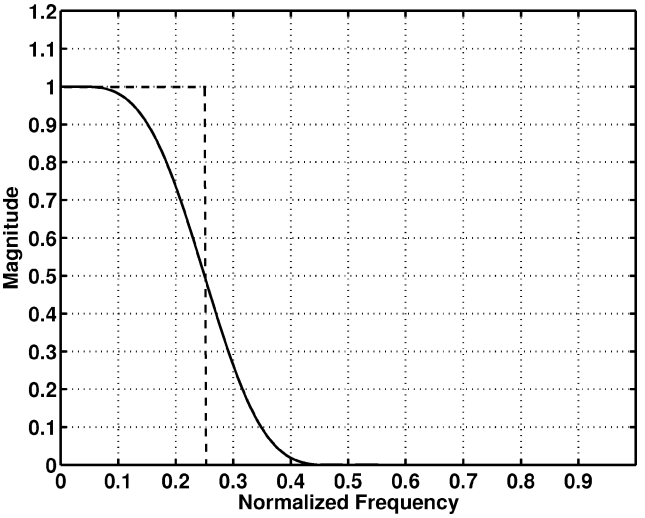

Fig. 8 $N = 21$, **cutoff frequency = 0.25: – – –, ideal filter response and ——, filter response of filter designed with window method using a Kaiser window.**

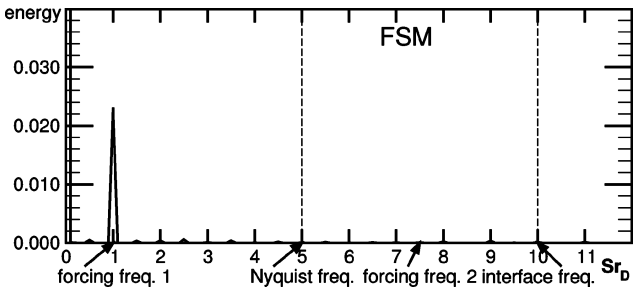

Fig. 9 Energy spectrum at interface plane of downstream domain with use of FSM designed filter (Fig. 7).

show the desired results (Figs. 9 and 10). The long-wave perturbation at $Sr = 1.0$, the frequency that is desired to be transmitted, can be found in the downstream domain without a loss of energy. Because the filters have eliminated the high-frequency perturbation before the actual sampling process, no aliasing can be observed. A comparison with the unfiltered spectrum shows that the energy of aliased frequency is reduced by 99.6% using the FSM method and by 99.7% for using the Kaiser window.

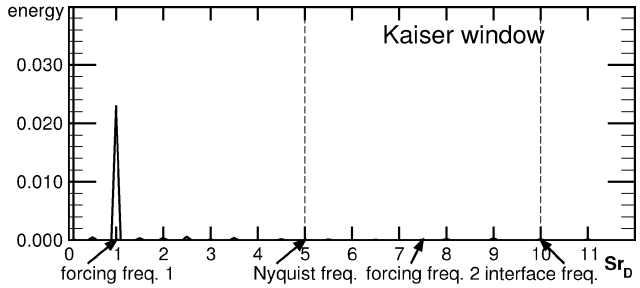

Fig. 10 Energy spectrum at interface plane of downstream domain with use of window method designed filter (Fig. 8).

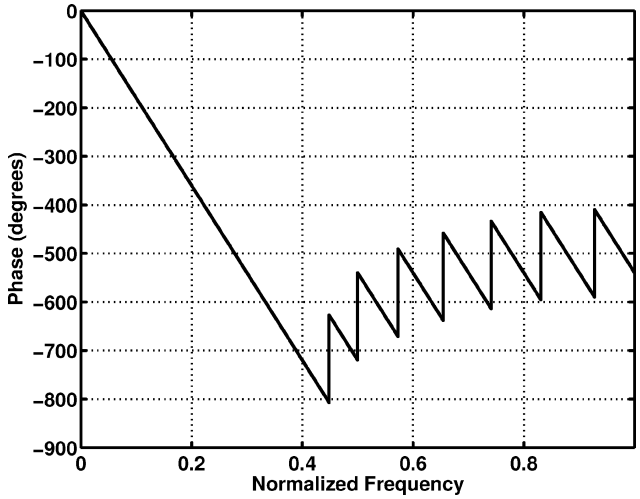

Fig. 11 Phase response of filter designed with window method using a Kaiser window, $N = 21$.

Whereas for the current test case the results of both filters are nearly identical, more complex test cases may require the choice of a filter based on the filter response. These results show that digital filters can be used to improve the quality of the signal taken from LES data to correct the amplitude response and attenuate aliasing.

C. Temporal Filter: Phase Response

The application of these filters have a major drawback. Figure 11 shows the phase response of both filters. The phase response is linear in the passing frequency range. This translates to a constant time delay of

$$\Delta t = (N-1)/2 \cdot f_{\text{sample}} \tag{4}$$

with which the signal coming from the upstream flow solver arrives in the downstream flow domain. The time delay can be minimized by decreasing the order of the filter, but the filters presented here with an order of $N = 21$ are the minimum order for a filter with an acceptable quality of amplitude response. If unsteady coupling effects are investigated, this time delay introduced by the filter is usually not acceptable.

Because the phase delay is unavoidable using these temporal filters, the application of these filters is limited to the following: most unsteady RANS flow solvers for turbomachinery applications do not claim to compute a truly unsteady flow but an ensemble average or a phase average. In phase-averaged flows, a number of averages of the flow are taken in relation to the phase of a base frequency f_{base}, which is tied to the rotational speed of the turbomachinery. When it is assumed that the LES delivers data to a RANS flow solver computing phase averages, the LES flow solver can compute phase averages on the basis of the LES data at the interface. Then, a filter is designed that creates the time delay for one full period of the base frequency. Here, the advantage of a linear phase response of a FIR filter is apparent: The linear phase response translates to a constant time delay that can be controlled by the order of the filter. The order of the filter is then determined by

$$N = 2 \cdot (f_{\text{sample}}/f_{\text{base}}) + 1 \tag{5}$$

Although this procedure might be working for a number of applications, most unsteady LES/RANS computations will neither tolerate the time delay nor the usage of phase averages at the interface.

VI. Spatial Filters

A. Definition

The major reason why temporal filters are creating a time delay is the lack of information of the signal in the future. For fluid flow, the Taylor hypothesis can be used to translate temporal to spatial information. The Taylor hypothesis can be written as

$$\frac{\partial .}{\partial t} = -u_c \frac{\partial .}{\partial x} \tag{6}$$

with u_c being the local convection velocity in the x direction. The Taylor hypothesis is valid if the Reynolds number is high and the flow is locally in the x direction. The temporal filter then becomes the spatial filter

$$r(t_k) = \sum_{n=0}^{N} b_n s(x_{k-n}) \tag{7}$$

with

$$x_n - x_{n-1} = u_c / f_{\text{sample}} \tag{8}$$

Instead of using the time history of the signal, the downstream development is sampled. Unlike the case of the temporal filters, where the time history of the interface points have to be stored, no additional memory is necessary for the spatial form of the filter.

So far, the phase delay is still present, unless the origin of the filter is shifted upstream placing the filter centrally around the desired interface point:

$$x_{0,\text{new}} = x_{0,\text{old}} - [(N-1)/2](u_c/f_{\text{sample}}) \tag{9}$$

Here, the location of the sampling points is defined by the sampling frequency. In many flow solvers, especially when using structured meshes, it may be of advantage to define the sampling frequency on the mesh spacing. The locations of the sampling points are then defined as points on the mesh and the sampling frequency by the distance of the points:

$$f_{\text{sample}} = u_c/\Delta x \tag{10}$$

The advantage of this definition is mainly of practical nature because it is easier to retrieve data from these points. Furthermore, no error due to aliasing in the presampling process is introduced because the sampling points resolve the entire spectrum on the given mesh.

The disadvantage of this definition of the sampling points is the independence of the sampling frequency from the interface frequency. A variation of the RANS time step (and hence, a variation of the interface frequency) requires a new definition of the filter because the desired cutoff frequency has changed although the sampling frequency remained constant.

For the current study, the spacing of mesh points in the axial direction is $\Delta x = 3D/128$. With $u_c = U_{\text{bulk}} = 1.0$, this results in a Strouhal number $Sr_{\text{sample}} = 42.67$. The cutoff frequency of $Sr = 5.0$ results in a normalized cutoff frequency $f_{\text{cutoff}} = 0.117$.

The number of sampling point is limited to $N = 17$. A small number of sampling points is desirable because the Taylor hypothesis loses validity with increasing distance from the interface point. Furthermore, the extent of the spatial filter is sought to be small for several reasons. First, in geometries more complex than the current pipe flow, the spatial filter has to be put into an area where the flow is nearly parallel and has a nearly constant convection velocity over the spatial extent of the filter. This may not be the case over a large

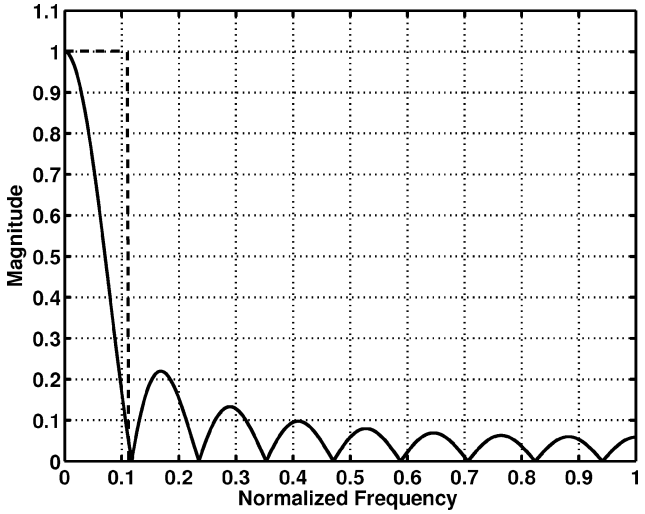

Fig. 12 $N = 17$: – – –, ideal filter response and ——, amplitude response of spatial filter based on a running average.

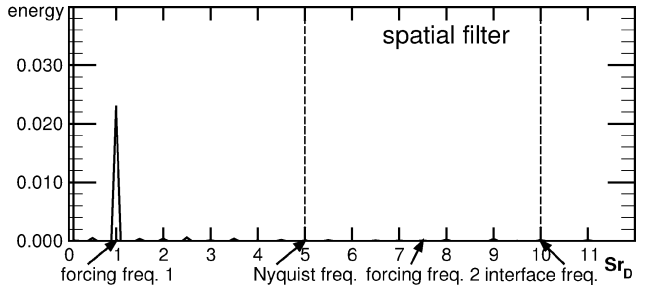

Fig. 13 Energy spectrum at interface plane of downstream domain; spatial running average filter (Fig. 12) used.

portion of the flow. Second, in parallel computations, the extent of a spatial filter may be larger than the extent of the flowfield computed on a single processor, so that interactions between parallel processors may be necessary.

Because it is rather difficult to design a filter with a low cutoff frequency, such as $f_{\text{cutoff}} = 0.117$, on the basis of few sampling points, a running average filter is employed ($b_n = 1/N$). This is the only filter that could ensure an amplitude response of unity at the mean flow. The resulting filter response can be seen in Fig. 12.

B. Spatial Filter: Amplitude Response

The spatial filter is implemented in the upstream flow solver computing the pipe flow. The integrated computation is performed and the received signal at the inlet of the downstream flow solver examined (Fig. 13). It can be seen that the low-frequency perturbation has passed the interface, although, due to the filtering, it has lost some energy (≈3%). The high-frequency perturbation has been filtered out sufficiently so that aliasing is successfully suppressed. In comparison to the unfiltered spectrum, the aliased frequency is attenuated by 99.1%.

C. Spatial Filter: Phase Response

The phase delay of this filter can be expressed as a constant time delay Δt, which is a sum of the filter time delay and the time correction by the shift of the origin Eq. (9),

$$\Delta t_{\text{total}} = \Delta t_{\text{filter}} + \Delta t_{\text{origin shift}} \tag{11}$$

The filter time delay Δt_{filter} is defined corresponding to Eq. (4). The time correction due to the shift of the origin upstream is given by

$$\Delta t_{\text{origin shift}} = \Delta x/u_c = -[(N-1)/2](u_c/f_{\text{sample}})(1/u_c) \tag{12}$$

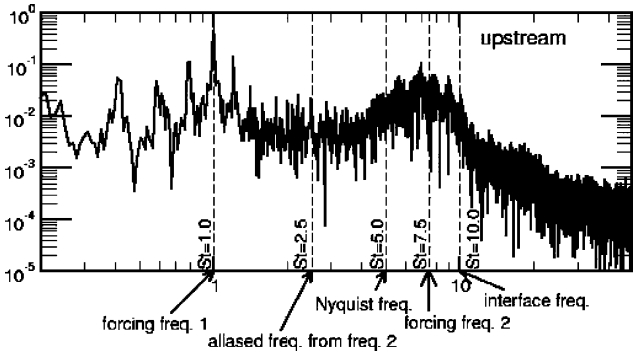

Fig. 14 Energy spectrum at interface: original signal in the upstream domain.

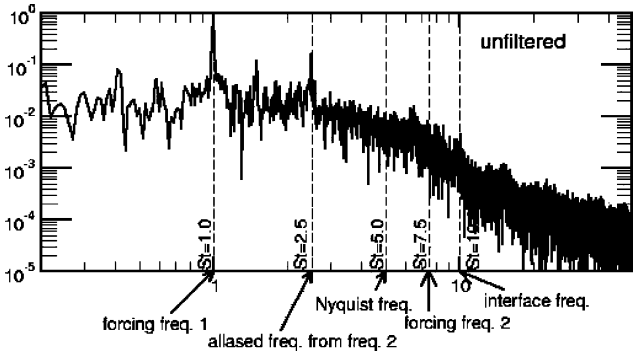

Fig. 15 Energy spectrum at interface: downstream solution without filtering.

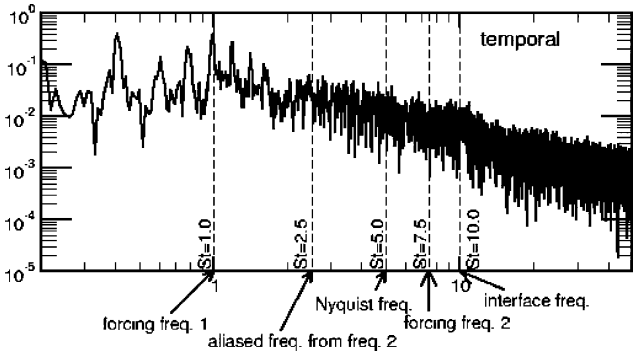

Fig. 16 Energy spectrum at the interface: downstream solution using temporal filter (Kaiser window).

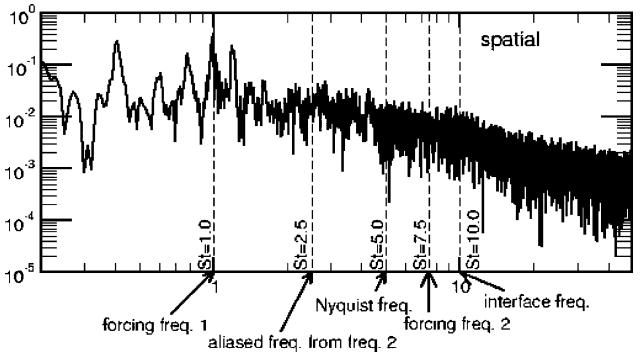

Fig. 17 Energy spectrum at the interface: downstream solution using spatial filter.

Equation (11) then becomes

$$\Delta t_{\text{total}} = \frac{N-1}{2 \cdot f_{\text{sample}}} - \frac{N-1}{2}\frac{1}{f_{\text{sample}}} = \mathbf{0} \tag{13}$$

The zero time delay ensures a true phase transfer of a given perturbation.

This result shows, that antialiasing with spatial filters is possible, allowing the proper transfer of amplitude and phase of a given long-wave perturbation and, hence, allowing for a true unsteady coupling between LES and RANS flow solvers.

VII. Filtering: Application to Turbulent Flows

To demonstrate the filtering procedures on turbulent flows, the computations are repeated using a turbulent pipe flow with a Reynolds number of $Re = 1.5 \times 10^4$. For both parts of the domain, LES flow solvers are used.

Because the inflow of the upstream pipe has to be turbulent, the inflow was generated by a separate LES computation of a periodic pipe flow with $Re = 1.5 \times 10^4$ and $S = 0.15$. The outflow plane of this computation is recorded into a database that is used as inflow for the actual LES computation.[17]

As in the laminar case, the swirl velocity is periodically excited. Here, the mean swirl velocity is modulated, whereas the turbulent fluctuations are left untouched. Because the propagation of a convective wave is disturbed by the turbulence, the upstream pipe is shortened by $1.5D$ so that the inlet plane is $0.5D$ upstream of the interface plane. This allows to obtain a clearer signal from the forcing at the interface plane.

The solution of the upstream flow solver is filtered at the appropriate plane using the RANS time step $\Delta\tau$. Inflow boundary conditions for the downstream LES flow solver are then generated using the database method described in Ref. 18. A database of turbulent flow data generated by a turbulent pipe flow simulation is used and scaled to satisfy the mean velocity and velocity fluctuations provided by the upstream flow solver. The database is generated by an LES computation of a periodic pipe at a higher Reynolds number $Re = 3 \times 10^4$ to point out differences in the high-frequency spectrum in the upstream and downstream domains.

Figure 14 shows the resulting energy spectrum in the upstream domain. The lower forcing frequency can be easily identified. The high-frequency forcing is disturbed by the turbulence and is less distinct. However, in the unfiltered downstream spectrum shown in Fig. 15, aliasing of the second frequency can be easily observed.

Applying a temporal filter to the upstream LES computation suppresses the aliasing successfully (Fig. 16). Some differences in the high-frequency spectrum between upstream and downstream domains can be observed. These are due to the reconstruction of high-frequency turbulence using a database in the downstream domain.

The use of a spatial filter yields essentially the same result as a temporal filter. This is shown in Fig. 17.

VIII. Conclusions

In integrated LES/RANS computations, the higher temporal resolution of the flow in the LES domain may lead to aliasing errors when sampling the data for the RANS flow solver using a larger time step. This problem is similar to the aliasing problem in experiments, where a continuous signal is digitally sampled and where antialiasing is achieved with low-pass filtering before the sampling. In the present study, we demonstrated the occurrence of such aliasing effects in coupled simulations running at different time steps. The application of digital filters before the sampling process has been proposed to achieve antialiasing.

The effects of two different digital filters of the order $N = 21$ are shown, and both filters are able to decrease aliasing by more than 99% for the chosen test case of a periodically perturbed pipe flow. However, a large phase delay is introduced by the filter, which makes it unsuitable for a truly unsteady coupling of LES and RANS flow solvers.

To avoid the phase delay caused by the digital filter, the temporal filters can be transformed into spatial filters using the Taylor hypothesis. It is demonstrated that the spatial formulation of the digital filter is able to attenuate aliasing substantially, while preserving the phase information. This makes this filter formulation a suitable antialiasing method for coupled RANS/LES computations.

The identification of the aliasing problem in integrated RANS/LES computations and its solution using spatial filters is an important step toward truly unsteady flow predictions using multicode RANS/LES flow simulations.

Appendix: Digital Filter Design

Digital filter design, especially low-order design, is currently more an art than an exact science. The minimum specifications for a digital filter vary from application to application. For coupled RANS/LES computations, the temporal digital filters are designed using a minimum number of coefficients and with a filter response of unity at 0 Hz to ensure the conservation of mean momentum. Here, two different filters are presented. One is derived mathematically from the desired filter response and is the basis for all filters. The other filter improves the filter response by employing a window function.

A. FSM

The first filter is designed using the FSM.[19] The coefficients can be derived from

$$b_n = \frac{1}{2\pi}\int_{2\pi} H(\lambda)[\cos(m\lambda) + j\sin(m\lambda)]\,\mathrm{d}\lambda \tag{A1}$$

with

$$m = n - [(N-1)/2] \tag{A2}$$

and with $H(\lambda)$ being the desired filter response and λ the normalized frequency, which is here normalized to the presampled frequency. The optimal filter response would have a cutoff frequency of $\frac{1}{2} \cdot f_{\text{interface}}$. The presampling frequency is chosen here twice the interface frequency, which results in a cutoff frequency $\lambda_{\text{cutoff}} = \frac{1}{4}$. Equation (A1) then becomes

$$b_n = \frac{1}{2\pi}\int_{\pi/4}^{\pi/4} \cos(m\lambda)\,\mathrm{d}\lambda + j\frac{1}{2\pi}\int_{\pi/4}^{\pi/4} \sin(m\lambda)\,\mathrm{d}\lambda \tag{A3}$$

The second integrand is zero because the integrand is an odd function and the limits of the integration are symmetric. Equation (A3) then becomes

$$b_n = \frac{\sin(m\lambda)}{2m\pi}\bigg|_{\lambda=-\pi/4}^{\lambda=\pi/4} = \frac{\sin[m(\pi/4)]}{m\pi} \tag{A4}$$

Please note that the definition of the filters does not include the knowledge of the actual sampling frequency, but only the cutoff frequency relative to the sampling frequency. This means that, if the interface frequency is changed, the filters will adapt automatically. The filter coefficients for $N = 21$ can be found in Table A1.

The filter response of this filter is shown in Fig. 7. The deviations of the actual filter response from the ideal filter response are due to the low number of filter coefficients. Most notably, an amplification

Table A1 Coefficients of the filter defined by Eq. (A4)

Coefficient	Value
b_0, b_{20}	0.0311536
b_1, b_{19}	0.0244766
b_2, b_{18}	−0.0000006
b_3, b_{17}	−0.0314696
b_4, b_{16}	−0.0519226
b_5, b_{15}	−0.0440576
b_6, b_{14}	0.0000006
b_7, b_{13}	0.0734296
b_8, b_{12}	0.1557666
b_9, b_{11}	0.2202866
b_{10}	0.2446776

Table A2 Coefficients of the filter using a Kaiser window

Coefficient	Value
b_0, b_{20}	0.0004736
b_1, b_{19}	0.0013386
b_2, b_{18}	−0.0000006
b_3, b_{17}	−0.0069236
b_4, b_{16}	−0.0179856
b_5, b_{15}	−0.0217416
b_6, b_{14}	0.0000006
b_7, b_{13}	0.0583416
b_8, b_{12}	0.1425086
b_9, b_{11}	0.2189896
b_{10}	0.2500006

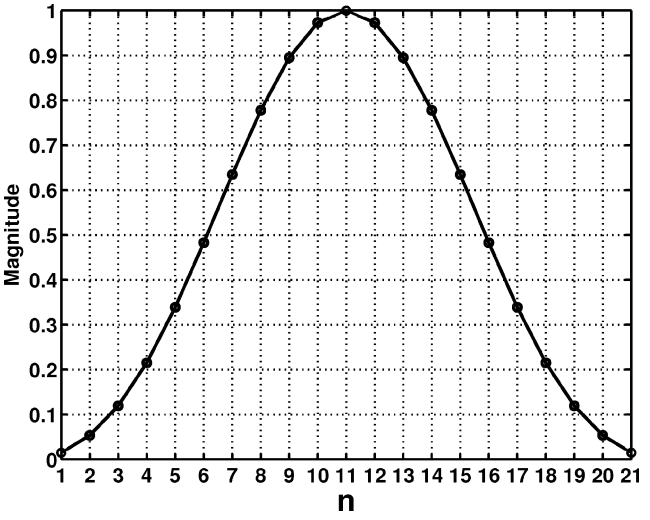

Fig. A1 Kaiser window used to improve filter respose, $N = 21$ and $\beta = 6$.

close to the cutoff frequency can be observed. This amplification is called Gibb's effect.

B. Window Method

The second filter used in this study uses a window method to smoothen the filter response. One of the major shortcomings of the FSM is the assumption that the signal is periodic. This creates some problems due to a discontinuity at the end and at the beginning of the recorded signal. One possibility to dampen this effect is to use window functions given by

$$r(t_k) = \sum_{n=0}^{N} b_n w_n s(t_{k-n}) \tag{A5}$$

with w_n being the window function. Some of the most common window functions are the Hann, Hamming, Parzen, or Kaiser windows (see Ref. 20). The choice of the appropriate window method is subjective and depends on the preferences of the designer. Currently, a number of filter design tools are available, which allow the investigation of the effect of a given window to the filter response. Here, the commercial package MATLAB® has been used.

Applying several windows to the filter ($N = 21$) results in varying filter responses. Some filters are not able to attenuate Gibb's phenomenon completely (such as the Hann and Hamming window). Others disturb the low-frequency spectrum significantly (such as the Parzen window) for the given order of the filter. Here, as a compromise, the Kaiser window was chosen (Fig. A1).

The window function is usually combined with the filter coefficients, which leads to a new set of coefficients provided in Table A2.

This filter has been designed to work under the current circumstances, but may have to be adapted for other applications, most notably, when a larger number of filter coefficients can be used.

Acknowledgment

The support by the U.S. Department of Energy under the Advanced Scientific Computing program is gratefully acknowledged.

References

[1]Davis, R., Yao, J., Clark, J. P., Stetson, G., Alonso, J. J., Jameson, A., Haldeman, C., and Dunn, M., "Unsteady Interaction Between a Transsonic Turbine Stage and Downstream Components," American Society of Mechanical Engineers, ASME Paper GT-2002-30364, June 2002.

[2]Veynante, D., and Poinsot, T., "Reynolds Averaged and Large Eddy Simulation Modeling for Turbulent Combustion," *New Tools in Turbulence Modelling*, ed. physique, Springer, Berlin, 1996, Chap. 5, pp. 105–140.

[3]Moin, P., and Apte, S., "Large-Eddy Simulation of Realistic Gas Turbine Combustors," AIAA Paper 2004-0330, Jan. 2004.

[4]Trenberth, K. E., *Climate System Modeling*. Cambridge Univ. Press, New York, 1992. Chap. 9.

[5]Adamidis, P., Beck, A., Becker-Lemgau, U., Ding, Y., Franzke, M., Holthoff, H., Laux, M., Müller, A., Münch, M., Reuter, A., Steckel, B., and Tilch, R., "Steel Strip Production—A Pilot Application for Coupled Simulation with Several Calculation Systems," *Journal of Materials Processing Technology*, Vol. 80–81, Aug. 1998, pp. 330–336.

[6]Spalart, P. R., "Trends in Turbulence Treatments," AIAA Paper 2000-2306, June 2000.

[7]Batten, P., Goldberg, U., and Chakravarthy, S., "LNS—An Approach Towards Embedded LES," AIAA Paper 2002-0427, Jan. 2002.

[8]Schlüter, J. U., Wu, X., Kim, S., Alonso, J. J., and Pitsch, H., "Integrated RANS-LES Computations of Gas Turbines: Compressor–Diffuser," AIAA Paper 2004-0369, Jan. 2004.

[9]Shankaran, S., Liou, M.-F., Liu, N.-S., Davis, R., and Alonso, J. J., "A Multi-Code-Coupling Interface for Combustor/Turbomachinery Simulations," AIAA Paper 2001-0974, Jan. 2001.

[10]Schlüter, J. U., Shankaran, S., Kim, S., Pitsch, H., Alonso, J. J., and Moin, P., "Integration of RANS and LES Flow Solvers for Simultaneous Flow Computations," AIAA Paper 2003-0085, Jan. 2003.

[11]Schlüter, J., Pitsch, H., Moin, P., Shankaran, S., Kim, S., and Alonso, J., "Towards Multi-Component Analysis of Gas Turbines with CFD: Integration of RANS and LES Flow Solvers," American Society of Mechanical Engineers, ASME GT-2003-38350, June 2003; also Schlüter, J. U., Wu, X., Kim, S., Alonso, J. J., and Pitsch, H., "A Framework for Coupling Reynolds-Averaged with Large Eddy Simulations for Gas Turbine Applications," *Journal of Fluids Engineering* (submitted for publication).

[12]Pierce, C., and Moin, P., "Large Eddy Simulation of a Confined Coaxial Jet with Swirl and Heat Release," AIAA Paper 98-2892, June 1998.

[13]Akselvoll, K., and Moin, P., "Large-Eddy Simulation of Turbulent Confined Coannular Jets," *Journal of Fluid Mechanics*, Vol. 315, 1996, pp. 387–411.

[14]Germano, M., Piomelli, U., Moin, P., and Cabot, W., "A Dynamic Subgrid-Scale Eddy Viscosity Model," *Physics of Fluids A*, Vol. 3, No. 7, 1991, pp. 1760–1765.

[15]Moin, P., Squires, K., Cabot, W., and Lee, S., "A Dynamic Subgrid-Scale Model for Compressible Turbulence and Scalar Transport," *Physics of Fluids A*, Vol. 3, No. 11, 1991, pp. 2746–2757.

[16]Schlüter, J. U., Pitsch, H., and Moin, P., "Outflow Conditions for Integrated Large Eddy Simulation/Reynolds-Averaged Navier–Stokes Simulations," *AIAA Journal*, Vol. 43, No. 1, 2005, pp. 156–164.

[17]Pierce, C. D., and Moin, P., "Method for Generating Equilibrium Swirling Inflow Conditions," *AIAA Journal*, Vol. 36, No. 7, 1998, pp. 1325–1327.

[18]Schlüter, J. U., Pitsch, H., and Moin, P., "Large Eddy Simulation Inflow Conditions for Coupling with Reynolds-Averaged Flow Solvers," *AIAA Journal*, Vol. 42, No. 3, 2004, pp. 478–484.

[19]Rorabaugh, C. B., *Digital Filter Designer's Handbook*, 2nd ed., McGraw–Hill, New York, 1997.

[20]Williams, C. S., *Designing Digital Filters*, Prentice–Hall, Upper Saddle River, NJ, 1986, Chap. 3.

R. So
Associate Editor